Dynamic role of coupled-channel wave phases on the structural determination of angular distributions

Min-Ho Lee* and Nark Nyul Choi†
Department of Physics, Kumoh National University of Technology, Kumi 730-701, Korea

Sung-Ho Suck Salk‡
Department of Physics, Pohang University of Science Technology, Pohang 790-784, Korea
(Received 7 August 1998)

It is still a question of interest why the distorted-wave Born approximation theory predicts well the structure of the angular distributions particularly at low energies, in good agreement with the coupled-channel wave theory. The phases of the coupled-channel waves are found to be crucially important in determining the structures of the angular distributions. The phases of coupled-channel wave functions are shown to be close to the phase of the entrance channel in the classically forbidden region at low energies, thus allowing agreement between the two theories. [S1050-2947(99)01803-X]

PACS number(s): 34.50.Lf

I. INTRODUCTION

For the past two or three decades there has been a unceasing interest in the study of rearrangement collisions (reactive scattering processes) involving atoms and molecules. For the $H+H_2$ benchmark exchange reaction, much effort has been made to obtain the accurate dynamical reaction information by performing rigorous calculations of cross sections, thermal rate constants, and state-to-state transition probabilities of reactive collision process near the threshold region, where the quantum-mechanical effects such as tunneling and resonances are important. For this purpose, various exact quantum-mechanical methods have been developed; they are the exact close-coupling methods [1–3], the *S*-matrix version of the Kohn-variational principle [4], the log-derivative version of the Kohn-variational principle [5], the method of discrete variable representation with absorbing boundary condition [6], etc. For computational efficiency, various reliable approximations [e.g., the single-channel distorted-wave Born approximation (DWBA) [7–10], the coupled-channel-wave (multichannel distorted-wave) Born approximation (CCBA) [11–15], the infinite-order sudden approximation [16], etc. [17]] have been proposed.

Among the approximation methods the DWBA and CCBA have been frequently used for the study of atom–diatomic-molecule reactive collisions at low collision energies [18,19]. In the DWBA, coupling between channels is not taken into account. The DWBA seems to describe well the relative (but not absolute) magnitudes of the integrated cross sections, the angular distributions [20], and the product rotational-vibrational distributions [14,21,22]. The DWBA is thus a useful tool for a qualitative description, although not so good for quantitative accuracy. Earlier, comparisons between the DWBA and the exact close-coupling calculations were reported [19,20]. These studies showed that the effect of coupling strongly affects the absolute magnitude of the cross section, even at low energies, but not the relative angular distribution. To take into account the effects of coupling to inelastic channels, the CCBA method was proposed [12,14,15]. The coupled-channel (CC) wave functions describe the elastic and inelastic scattering in each arrangement. The CCBA calculations are known to be in excellent agreement with the exact ones at relatively low energies (near the threshold region) [1,14].

However, it is still an unanswered problem why the DWBA theory works surprisingly well in the prediction of the relative angular distributions at low collision energies. Only formal differences between the CCBA and DWBA methods were elucidated earlier [23]. Recently, in order to resolve why the DWBA, which allows only a single channel, is a useful tool to explore the structures of angular distributions at such low energies we have numerically investigated connections between the CCBA and DWBA and showed that constancy of the computed phases of CC wave functions is important for structural agreement in angular distributions [24]. In the present paper, employing a perturbative approach, we present a full explanation of reasons why such constancy often occurs and why the phases of CC waves are close to the phase of the entrance channel.

The CCBA transition amplitude is briefly described in Sec. II. In Sec. III we demonstrate the importance of the CC wave phases in determining the angular distributions. In addition, we present the numerical results on the phases of CC waves with emphasis on their characteristics. In Sec. IV we introduce a perturbative expansion of CC waves and the coupling potential matrix elements are investigated. In Sec. V the phase of the distorted-wave (DW) Green's function is proved to be zero and the phases of CC waves are investigated on the basis of the perturbative approach.

II. STATE-TO-STATE REACTIVE TRANSITION AMPLITUDES

The differential cross section for the state-to-state reactive scattering $A+BC(n_a,j_a)\rightarrow AB(n_b,j_b)+C$ is written as

*Electronic address: mhlee@m700.kumoh.ac.kr
†Electronic address: nnchoi@molecule.kumoh.ac.kr
‡Electronic address: salk@postech.ac.kr

$$\left(\frac{d\sigma}{d\Omega}\right)_{n_b j_b, n_a j_a} = \frac{1}{2j_a+1}\frac{\mu_{A,BC}\mu_{C,AB}}{4\pi^2}\frac{K_b}{K_a} \times \sum_{m_b m_a} |T_{n_b j_b m_b, n_a j_a m_a}(\Omega)|^2, \quad (1)$$

where the reactive transition amplitude $T_{n_b j_b m_b, n_a j_a m_a}(\Omega)$ can be expressed as [12,18]

$$T_{n_b j_b m_b, n_a j_a m_a}(\Omega) = -\sum 4\pi^2 i^{L_a - L_b}\frac{\sqrt{v_b v_a}}{K_b K_a}\langle j_b L_b m_b M_b | JM\rangle \times \langle JM | j_a L_a m_a M_a\rangle Y_{L_b M_b}(\hat{K}_b) Y^*_{L_a M_a}(\hat{K}_a) \times T^J_{n_b j_b L_b, n_a j_a L_a}. \quad (2)$$

Here $n_a(n_b)$, $j_a(j_b)$, and $m_a(m_b)$ are, respectively, the vibrational, rotational, and polarizational quantum numbers of the reactant (product) molecule. $\mu_{A,BC}(\mu_{C,AB})$, $\mathbf{K}_a(\mathbf{K}_b)$, and $v_a(v_b)$ are, respectively, the reduced mass, the wave vector, and the velocity for the relative motion in the initial (final) arrangement. J and M are the total angular momentum and its projection quantum numbers, respectively. L_a (L_b) is the orbital angular momentum of the initial (final) arrangement and M_a (M_b) its projection quantum number. Ω is the solid angle of the wave vector $\mathbf{K}_b$ with respect to the wave vector $\mathbf{K}_a$. It can be seen from Eq. (2) that the essential physics of $T_{n_b j_b m_b, n_a j_a m_a}(\Omega)$ as a function of m_b, m_a, and Ω is ultimately understood from the nature of $T^J_{n_b j_b L_b, n_a j_a L_a}$. The latter contains information on important dynamics in association with the angular momentum J, L_b, and L_a and possesses rotational invariance, revealing the complete dynamic properties of reactive collision processes.

In the framework of the CCBA, $T^J_{n_b j_b L_b, n_a j_a L_a}$ is written as

$$T^J_{n_b j_b L_b, n_a j_a L_a} = \int dR_b\, dR_a\, R_b R_a \sum_{n'_b j'_b L'_b, n'_a j'_a L'_a} \chi^{J(-)*}_{n'_b j'_b L'_b, n_b j_b L_b} \times (R_b) K^J_{n'_b j'_b L'_b, n'_a j'_a L'_a}(R_b, R_a)\chi^{J(+)}_{n'_a j'_a L'_a, n_a j_a L_a}(R_a). \quad (3)$$

Here $K^J_{n'_b j'_b L'_b, n'_a j'_a L'_a}(R_b, R_a)$ is the reaction kernel that depends on the total angular momentum J. This kernel represents the intrinsic nature of rearrangement collisions involving transitions from the intermediate channels $\{n'_a j'_a L'_a J\}$ in the initial arrangement to the intermediate channels $\{n'_b j'_b L'_b J\}$ in the final arrangement. It is given by [12,14]

$$K^J_{n'_b j'_b L'_b, n'_a j'_a L'_a} = \int d\hat{R}_b\, d\hat{R}_a \frac{u_{n'_b j'_b}(r_b)}{r_b}\mathcal{Y}^{JM*}_{j'_b L'_b}(\hat{\mathbf{r}}_b, \hat{\mathbf{R}}_b) \times \left[U_\alpha(R_b, R_a, \hat{\mathbf{R}}_b\cdot\hat{\mathbf{R}}_a)\frac{u_{n'_a j'_a}(r_a)}{r_a}\mathcal{Y}^{JM}_{j'_a L'_a}(\hat{\mathbf{r}}_a, \hat{\mathbf{R}}_a) - \sum_{n''_a, j''_a, L''_a}\frac{u_{n''_a j''_a}(r_a)}{r_a}\mathcal{Y}^{JM}_{j''_a L''_a}(\hat{\mathbf{r}}_a, \hat{\mathbf{R}}_a) \times [U_\alpha(R_a)]^J_{n''_a j''_a L''_a, n'_a j'_a L'_a}\right]. \quad (4)$$

$\mathbf{R}_a$ $(\mathbf{R}_b)$ is the channel radius vector from the center of mass of the diatomic molecule BC (AB) to the atom A (C) and $\mathbf{r}_a$ $(\mathbf{r}_b)$ is the interatomic displacement of the diatomic molecule in the initial (final) arrangement. $\chi^{J(+)}_{n'_a j'_a L'_a, n_a j_a L_a}(R_a)$ and $\chi^{J(-)}_{n'_b j'_b L'_b, n_b j_b L_b}(R_b)$ are the outgoing and incoming CC wave functions corresponding to the initial and final arrangements, respectively. $u_{n'_a j'_a}(r_a)$ and $u_{n'_b j'_b}(r_b)$ are the molecular wave functions in the initial and final arrangements. $U_\alpha(R_b, R_a, \hat{\mathbf{R}}_b\cdot\hat{\mathbf{R}}_a)$ describes the interaction between the projectile and the target. This interaction potential is set to be just the difference between the full three-body potential and the molecular potential in the initial arrangement. $[U_\alpha(R_a)]^J_{n''_a j''_a L''_a, n'_a j'_a L'_a}$ is the interaction matrix element $\langle n'_a j'_a L'_a | U_\alpha | n''_a j''_a L''_a\rangle^J$ that represents coupling between the intermediate channels $\{n''_a j''_a L''_a J\}$ and $\{n'_a j'_a L'_a J\}$. $\mathcal{Y}^{JM}_{j'_a L'_a}(\hat{\mathbf{r}}_a, \hat{\mathbf{R}}_a)$ is the bispherical harmonics [12,26]. The summation in Eq. (3) is over all the possible intermediate channels due to coupling with the entrance or exit channel. In the DWBA such intermediate (inelastic) channels are ignored, as is well known. The CC (or multichannel) wave functions $\chi^J_{n'_a j'_a L'_a, n_a j_a L_a}$, which describe the nonreactive scattering process in the initial arrangement, are obtained from the coupled differential equation

$$-\frac{1}{2\mu_{A,BC}}\left(\frac{d^2}{dR_a^2} - \frac{L'_a(L'_a+1)}{R_a^2} + k^2_{n'_a j'_a}\right)\chi^J_{n'_a j'_a L'_a, n_a j_a L_a}(R_a) + \sum_{n''_a, j''_a, L''_a}\langle n'_a j'_a L'_a | U_\alpha | n''_a j''_a L''_a\rangle^J \chi^J_{n''_a j''_a L''_a, n_a j_a L_a}(R_a) = 0, \quad (5)$$

where the wave numbers are given by $k^2_{n'_a j'_a} = 2\mu_{A,BC}(E - \epsilon_{n'_a j'_a})$ with the molecular energies $\epsilon_{n'_a j'_a}$.

III. IMPORTANCE OF COUPLED-CHANNEL WAVE PHASES FOR THE STRUCTURAL DETERMINATION OF ANGULAR DISTRIBUTIONS

To properly understand the physics of reactive transition, we focus on the transition amplitude of $T^J_{n_b j_b L_b, n_a j_a L_a}$ in Eq. (2) since it contains the dynamical information of the reaction. To the best of our knowledge, there has been no report on the explicit study of dynamic phase distributions involving the transition amplitude $T^{J,CCBA}_{n_b j_b L_b, n_a j_a L_a}$ for the purpose of explaining the cause of structural agreements in the predicted relative angular distributions between the DWBA and CCBA. Earlier, the shape of the relative angular distribution was discussed in terms of the examination of the reaction

TABLE I. $T^J_{n_b j_b J-1, n_a j_a J}$ in the CCBA and DWBA. Numbers in square brackets indicate powers of 10.

			Magnitude of T^J		Argument of T^J (in units of π)	
J	L_b	L_a	CCBA	DWBA	CCBA	DWBA
1	0	1	0.653[−02]	0.714[−03]	1.393	1.067
2	1	2	0.642[−2]	0.709[−3]	1.294	0.983
3	2	3	0.548[−2]	0.609[−3]	1.135	0.833
4	3	4	0.424[−2]	0.472[−3]	0.919	0.633
5	4	5	0.299[−2]	0.333[−3]	0.646	0.374
6	5	6	0.192[−2]	0.214[−3]	0.318	0.061
7	6	7	0.113[−2]	0.126[−3]	1.937	1.694
8	7	8	0.606[−3]	0.678[−4]	1.504	1.278
9	8	9	0.296[−3]	0.333[−4]	1.021	0.811
10	9	10	0.131[−3]	0.150[−4]	0.491	0.294
11	10	11	0.528[−4]	0.615[−5]	1.916	1.733
12	11	12	0.193[−4]	0.231[−5]	1.298	1.133

probability $|T^J_{n_b j_b L_b, n_a j_a L_a}|^2$ as a function of the total angular momentum $\boldsymbol{J}$ [14,15,18]. However, as can be seen from Eq. (2), the transition amplitude $T_{n_b j_b m_b, n_a j_a m_a}(\Omega)$ is expressed as a coherent sum of $T^J_{n_b j_b L_b, n_a j_a L_a}$. As the interference terms are determined by not only the magnitude distribution but also phase distributions, the phase distributions are expected to play an important role in determining the structure of angular distributions. In order to explicitly demonstrate the importance of the phase distribution, we compare the angular distributions resulting from two different phase distributions of $T^J_{n_b j_b L_b, n_a j_a L_a}$. In the first case, we choose the actual phase distribution obtained by the CCBA for the reaction $H+H_2(0,0) \rightarrow H_2(0,1)H+H$ (see Tables I and II). In the second case, the phase distribution is chosen arbitrarily. The actual magnitude distribution of $T^J_{n_b j_b L_b, n_a j_a L_a}$ is employed in both calculations of the the angular distributions. Even though the distributions of absolute magnitudes of $T^J_{n_b j_b L_b, n_a j_a L_a}$ are identical, the different phase distributions involving $T^J_{n_b j_b L_b, n_a j_a L_a}$ give quite different angular distributions as shown in Fig. 1. This explicitly shows that the structure of angular distribution is crucially determined by the phase distribution as well as by the magnitude distribution of $T^J_{n_b j_b L_b, n_a j_a L_a}$.

By choosing the Porter-Karplus potential-energy surface [25], we computed the transition amplitudes $T^{J,CCBA}_{n_b j_b L_b, n_a j_a L_a}$ and $T^{J,DWBA}_{n_b j_b L_b, n_a j_a L_a}$ for the reaction process $H+H_2(0,0) \rightarrow H_2(0,1)+H$ at a total energy of $E=0.5$ eV. Converged results were obtained by using the molecular basis sets $\{(n'_a, j'_a);\ n'_a=0,1,2,3$ and $j'_a=0,2,4,6\}$ for the initial arrangement and $\{(n'_b, j'_b);\ n'_b=0,1,2,3$ and $j'_b=1,3,5,7\}$ for the final arrangement. Satisfactory convergence in the predicted differential cross section was achieved with the maximum value of the total angular momentum being 12. At this energy the CCBA cross section was found to be in good agreement with the exact one [1,14]. Surprisingly, as shown in Tables I and II, the computed phases of $T^{J,DWBA}_{n_b j_b L_b, n_a j_a L_a}$ are in reasonable agreement with those of $T^{J,CCBA}_{n_b j_b L_b, n_a j_a L_a}$, except the common phase angle difference of $\sim 60°$. It is notable

TABLE II. $T^J_{n_b j_b J+1, n_a j_a J}$ in the CCBA and DWBA. Numbers in square brackets indicate powers of 10.

			Magnitude of T^J		Argument of T^J (in units of π)	
J	L_b	L_a	CCBA	DWBA	CCBA	DWBA
0	1	0	0.110[−1]	0.116[−2]	1.412	1.067
1	2	1	0.782[−2]	0.808[−3]	1.332	0.978
2	3	2	0.596[−2]	0.600[−3]	1.191	0.833
3	4	3	0.430[−2]	0.420[−3]	0.992	0.633
4	5	4	0.288[−2]	0.273[−3]	0.735	0.372
5	6	5	0.178[−2]	0.164[−3]	0.422	0.058
6	7	6	0.101[−2]	0.909[−4]	0.053	1.689
7	8	7	0.528[−3]	0.463[−4]	1.631	1.272
8	9	8	0.252[−3]	0.217[−4]	1.158	0.806
9	10	9	0.110[−3]	0.936[−5]	0.635	0.292
10	11	10	0.435[−4]	0.371[−5]	0.065	1.733
11	12	11	0.157[−4]	0.135[−5]	1.451	1.133
12	13	12	0.514[−5]	0.448[−6]	0.794	0.489

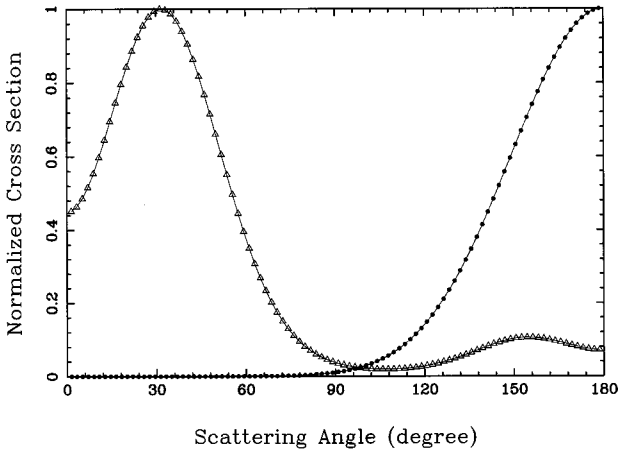

FIG. 1. Normalized cross sections for the actual phase distribution (●) and an arbitrarily chosen phase distribution (△) with the same magnitude distribution of $T^J_{n_a j_a L_a n_b j_b L_b}$.

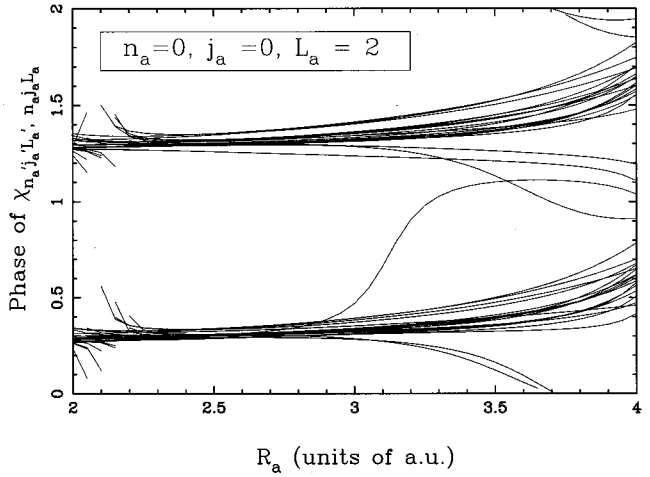

FIG. 2. Phase angles of all possible intermediate channels (coupled-channel wave functions) for the set of $J=2$, $n_a=0$, $j_a=0$, and $L_a=2$ in units of π. The number of available channels is 40 in this case.

that the common exponential factor arising from the common phase angle difference is extracted from the summation in Eq. (2) and is canceled during the process of computing the absolute magnitude square to obtain the differential cross section in Eq. (1). The predicted magnitudes of $T^{J,CCBA}_{n_b j_b L_b, n_a j_a L_a}$ are also in reasonable agreement with those of $T^{J,DWBA}_{n_b j_b L_b, n_a j_a L_a}$ except the common multiplication factor of ~ 10. This implies that coupling to inelastic channels enhances the absolute magnitude of the reactive cross section by 100 times larger than the value without the channel coupling.

It is readily seen from Eq. (3) that the dynamic (energy-dependent) phases of $T^J_{n_b j_b L_b, n_a j_a L_a}$ are determined by the phases of the CC waves $\chi^J_{n_a' j_a' L_a', n_a j_a L_a}$ and $\chi^J_{n_b' j_b' L_b', n_b j_b L_b}$. It is notable that the reaction kernel $K^J_{n_b' j_b' L_b', n_a' j_a' L_a'}$ is real valued. Investigating the distributions of the integrand of Eq. (3) in (R_b, R_a) space [24], we find that *the CC wave functions* $\chi^J_{n_a' j_a' L_a', n_a j_a L_a}$ *and* $\chi^J_{n_b' j_b' L_b', n_b j_b L_b}$ *in the classically forbidden region (that is, in the range* $2.3\ a.u. < R_a < 3.5\ a.u.$*) dominantly contribute to the transition amplitude* $T^J_{n_b j_b L_b, n_a j_a L_a}$. In this contributive region, the predicted phases of $\chi^J_{n_a' j_a' L_a', n_a j_a L_a}$ involving all possible intermediate channels $\{n_a' j_a' L_a'\}$ do not vary appreciably, as is shown in Fig. 2. Each curve represents the phase variation of CC waves as a function of the initial channel radius. To avoid typographical complexity, we avoid labeling each channel in the figure. We find that computed phases for all other initial channel show a similar trend. All the computed phases of the CC waves in a given initial channel $\{n_a j_a L_a\}$ are found to be nearly the same as the phase of the elastic channel wave $\chi^J_{n_a j_a L_a, n_a j_a L_a}$, allowing the maximum phase difference of 20° between the elastic and contributive intermediate channels. Further the magnitude of the phases are nearly independent of the channel radius R_a, particularly in the classically forbidden region of 2.3 a.u.$< R_a <$3.5 a.u. It is noted that, except the common phase angle difference of 30°, the weighted average of predicted phases of $\chi^{J,CCBA}_{n_a' j_a' L_a', n_a j_a L_a}$ is nearly the same as that of $\chi^{J,DWBA}_{n_a j_a L_a, n_a j_a L_a}$ at sufficiently low energies. To put it otherwise, it is important to realize that the memory of the initial (final) phase of the entrance (exit) channel is not lost during the nonreactive scattering at such low collision energies. This is one of the reasons why the structures of angular distributions between the DWBA and CCBA are found to be similar in the literature.

IV. PERTURBATIVE EXPANSION OF COUPLED-CHANNEL WAVES

The numerical results on the phases of the CC waves hint that a perturbative approach might be employed to understand these results. Decomposing the interaction matrix $\langle n_a' j_a' L_a' | U_\alpha | n_a'' j_a'' L_a'' \rangle^J$ into the diagonal (elastic) and off-diagonal (inelastic) parts, Eq. (5) can be rewritten as

$$\begin{aligned} &-\frac{1}{2\mu_{A,BC}}\left(\frac{d^2}{dR_a^2}-\frac{L_a'(L_a'+1)}{R_a^2}+k^2_{n_a' j_a'}\right. \\ &\qquad \left.-2\mu_{A,BC}\langle n_a' j_a' L_a' | U_\alpha | n_a' j_a' L_a' \rangle^J\right) \\ &\qquad \times \chi^J_{n_a' j_a' L_a', n_a j_a L_a}(R_a) \\ &= -\sum_{n_a'', j_a'', L_a''} \langle n_a' j_a' L_a' | U_\alpha | n_a'' j_a'' L_a'' \rangle^J (1 \\ &\qquad -\delta_{n_a', n_a''}\delta_{j_a', j_a''}\delta_{L_a', L_a''}) \chi^J_{n_a'' j_a'' L_a'', n_a j_a L_a}(R_a). \end{aligned} \tag{6}$$

Further, introducing the coupling potential matrix

$$V_{\tilde{n}_a', \tilde{n}_a''} \equiv \langle \tilde{n}_a' | U_\alpha | \tilde{n}_a'' \rangle^J (1-\delta_{\tilde{n}_a', \tilde{n}_a''}) \tag{7}$$

and the DW differential operator

$$\Delta_{\tilde{n}_a,\tilde{n}'_a}=-\frac{1}{2\mu_{A,BC}}\left(\frac{d^2}{dR_a^2}-\frac{L'_a(L'_a+1)}{R_a^2}+k^2_{n'_aj'_a}-2\mu_{A,BC}\langle\tilde{n}'_a|U_\alpha|\tilde{n}'_a\rangle^J\right)\delta_{\tilde{n}_a,\tilde{n}'_a}, \quad (8)$$

we rewrite Eq. (6) in the form of a matrix equation

$$\Delta\cdot\chi=-V\cdot\chi. \quad (9)$$

Here $\tilde{n}_a\equiv\{n_aj_aL_a\}$ was introduced for brevity. It is noted that V allows inelastic processes. That is, ignorance of V corresponds to the DWBA.

The perturbative solution $\chi^J_{\tilde{n}'_a,\tilde{n}_a}$ of Eq. (9) is

$$\chi=\chi^{0(+)}+\mathcal{G}^{(+)}V\chi^{0(+)}+\mathcal{G}^{(+)}V\mathcal{G}^{(+)}V\chi^{0(+)}+\cdots, \quad (10)$$

where $\chi^{0(+)}$ is the DW function that satisfies the elastic wave equation $\Delta\cdot\chi=0$ with an outgoing boundary condition. The DW Green's function $\mathcal{G}^{(+)}=-\Delta^{-1}$ is given by [28,29]

$$\mathcal{G}^{(+)}_{\tilde{n}_a,\tilde{n}'_a}(R_a,R'_a)=2\mu_{A,BC}\frac{\delta_{\tilde{n}_a,\tilde{n}'_a}}{W_{\tilde{n}_a}}\begin{cases}f_{\tilde{n}_a}(R_a)g_{\tilde{n}_a}(R'_a), & R_a<R'_a\\ g_{\tilde{n}_a}(R_a)f_{\tilde{n}_a}(R'_a), & R_a>R'_a.\end{cases} \quad (11)$$

Here $f_{\tilde{n}_a}(R_a)$ and $g_{\tilde{n}_a}(R_a)$ are, respectively, the regular and irregular solutions of the elastic wave equation $\Delta\cdot\chi=0$. They satisfy the asymptotic boundary conditions

$$f_{\tilde{n}_a}(R_a)\underset{R_a\to\infty}{\to}\begin{cases}\frac{1}{\sqrt{v_{\tilde{n}_a}}}[e^{-i(k_{\tilde{n}_a}R_a-L_{\tilde{n}_a}\pi/2)}-e^{i(k_{\tilde{n}_a}R_a-L_{\tilde{n}_a}\pi/2)}S^0_{\tilde{n}_a,\tilde{n}_a}] & \text{for open channels}\\ \frac{1}{\sqrt{v_{\tilde{n}_a}}}[e^{|k_{\tilde{n}_a}|R_a}-e^{-|k_{\tilde{n}_a}|R_a}S^0_{\tilde{n}_a,\tilde{n}_a}] & \text{for closed channels}\end{cases} \quad (12)$$

and

$$g_{\tilde{n}_a}(R_a)\underset{R_a\to\infty}{\to}\begin{cases}\frac{1}{\sqrt{v_{\tilde{n}_a}}}[e^{i(k_{\tilde{n}_a}R_a-L_{\tilde{n}_a}\pi/2)}] & \text{for open channels}\\ \frac{1}{\sqrt{v_{\tilde{n}_a}}}[e^{-|k_{\tilde{n}_a}|R_a}] & \text{for closed channels.}\end{cases} \quad (13)$$

The Wronskian $W_{\tilde{n}_a}$ is given by

$$W_{\tilde{n}_a}=f_{\tilde{n}_a}\frac{d}{dR_a}g_{\tilde{n}_a}-g_{\tilde{n}_a}\frac{d}{dR_a}f_{\tilde{n}_a}=\begin{cases}2i\mu_{A,BC} & \text{for open channels}\\ -2\mu_{A,BC} & \text{for closed channels.}\end{cases} \quad (14)$$

It is noted that $f_{\tilde{n}_a}(R_a)\equiv\chi^{0(+)}_{\tilde{n}'_a,\tilde{n}_a}\delta_{\tilde{n}'_a,\tilde{n}_a}$ by definition. The regular and irregular functions $f_{\tilde{n}_a}(R_a)$ and $g_{\tilde{n}_a}(R_a)$ for closed channels are real valued. This means that *the Green's functions $\mathcal{G}^{(+)}_{\tilde{n}_a,\tilde{n}_a}$ for closed channels are real valued.*

The perturbation potential in Eq. (10) is just the coupling potential V. For the $H+H_2$ reaction, the interaction potential U^α is invariant with respect to the reflection $\hat{\boldsymbol{r}}_a\cdot\hat{\boldsymbol{R}}_a\to-\hat{\boldsymbol{r}}_a\cdot\hat{\boldsymbol{R}}_a$. Hence we can expand it in a series of even-parity Legendre polynomials [1]

$$U^\alpha(r_a,R_a,\hat{\boldsymbol{r}}_a\cdot\hat{\boldsymbol{R}}_a)=\sum_{q=0}^{\infty}U^\alpha_{2q}(r_a,R_a)P_{2q}(\hat{\boldsymbol{r}}_a\cdot\hat{\boldsymbol{R}}_a), \quad (15)$$

where

$$U^\alpha_{2q}(r_a,R_a)=\frac{4q+1}{2}\int_{-1}^{1}U^\alpha(r_a,R_a,\hat{\boldsymbol{r}}_a\cdot\hat{\boldsymbol{R}}_a)\times P_{2q}(\hat{\boldsymbol{r}}_a\cdot\hat{\boldsymbol{R}}_a)d(\hat{\boldsymbol{r}}_a\cdot\hat{\boldsymbol{R}}_a). \quad (16)$$

Then the coupling potential matrix can be written as

$$V_{\tilde{n}'_a,\tilde{n}_a}(R_a)=\sum_{q=0}^{\infty}C_{2q}(j'_aL'_aj_aL_aJ)V^{(2q)}_{\tilde{n}'_a,\tilde{n}_a}(R_a), \quad (17)$$

where

$$C_\kappa(j'_aL'_aj_aL_aJ)=(-1)^{J+L_a+\kappa}[(2j'_a+1)(2L_a+1)]^{1/2}\langle j'_a\kappa00|j_a0\rangle\times\langle L_a\kappa00|L'_a0\rangle W(L_aj_aL'_aj'_a;J\kappa) \quad (18)$$

and

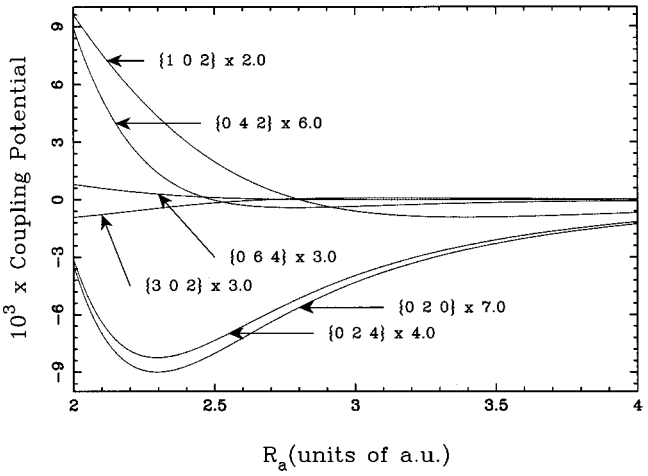

FIG. 3. Coupling potential matrix elements $V_{\tilde{n}_a',\tilde{n}_a}(R_a)$ between $\tilde{n}_a=\{002\}$ and $\tilde{n}_a'=\{020\}$, $\{024\}$, $\{042\}$, $\{064\}$, $\{102\}$, and $\{302\}$ in a.u. The scale factors indicated are the numbers by which the coupling potential matrix elements were multiplied before being plotted.

$$V^{(2q)}_{\tilde{n}_a',\tilde{n}_a}(R_a)=\langle u_{n_a'j_a'}(r_a)|U^{\alpha}_{2q}(r_a,R_a)|u_{n_aj_a}(r_a)\rangle. \quad (19)$$

The Racah coefficients W in Eq. (18) are expressed in the notation of Edmonds [27]. Since $C_{2q}(j_a'L_a'j_aL_aJ)=0$ for $j_a'+j_a$ odd or $L_a'+L_a$ odd, V does not couple even with odd rotational (orbital) channels. U^{α}, which represents the interaction between the target and the projectile, decreases as R_a^{-6} at large R_a. $U_0^{\alpha}(r_a,R_a)$ also decreases as R_a^{-6} by inheritance. The $2q$ pole of the interaction potential $U_{2q}^{\alpha}(r_a,R_a)$ with nonzero q measures the anisotropy. Accordingly, as q grows larger, $U_{2q}^{\alpha}(r_a,R_a)$ decreases more rapidly. This means that the coupling potential matrix element $V_{\tilde{n}_a',\tilde{n}_a}$ is mainly determined by the first nonzero term with $q=q_0$ in the series of Eq. (17) and that the channel coupling with smaller q_0 corresponds to a stronger one. In addition, for a fixed q_0, the smaller difference of the vibrational quantum numbers $\Delta n=n_a'-n_a$, the stronger channel coupling. In summary, *channels are most strongly coupled with their nearest neighbors* and the elements of the coupling potential matrix are monotonically decreasing functions of R_a at sufficiently large R_a. Numerical results of the coupling potential matrix elements are presented in Fig. 3, which is shown to be consistent with the arguments above.

V. EXAMINATION OF COUPLED-CHANNEL WAVE PHASES

To investigate the CC wave phases on the basis of the perturbative expansion (10) we plan to examine the phases and amplitudes of $f_{\tilde{n}_a}$,$g_{\tilde{n}_a}$, and $\mathcal{G}^{(+)}V\chi^{0(+)}$, including higher-order terms such as $\mathcal{G}^{(+)}V\mathcal{G}^{+}V\chi^{0(+)}$. To illustrate the procedure, we consider the case in which the entrance channel is specified by $\{n_a=0,j_a=0,L_a=2,J=2\}$ as an example.

First, we examine the phases and amplitudes of $f_{\tilde{n}_a}$ and $g_{\tilde{n}_a}$ for open channels. In the case of the present example, there are seven open channels that can be coupled to the entrance channel. As shown in Figs. 4 and 5, each of the complex regular functions $f_{\tilde{n}_a}$ is sinusoidal in the region of large R_a, has a maximum absolute magnitude (or modulus) near the classical turning point, and exponentially decreases in the classically forbidden region. This results from the repulsive nature of the effective elastic (distorting) potential

$$U^{eff}_{\tilde{n}_a,\tilde{n}_a}(R_a)\equiv\frac{L_a(L_a+1)}{2\mu_{A,BC}R_a^2}+\langle\tilde{n}_a|U|\tilde{n}_a\rangle, \quad (20)$$

as shown in Fig. 6. In particular, *the wave function $f_{\tilde{n}_a}$ in the classically forbidden region does not oscillate (no change in sign), its argument (phase) being constant in that region.* As the kinetic energy $k^2_{\tilde{n}_a}/2\mu_{A,BC}$ in the open channel decreases, the turning point quickly moves to large R_a. This is due to rapid broadening of the classical forbidden region, which is related to the shape of $U^{eff}_{\tilde{n}_a,\tilde{n}_a}(R_a)$ (see Fig. 6).

The magnitudes of the irregular functions $g_{\tilde{n}_a}$ are seen to be very large in the classically forbidden region. They exponentially decrease as R_a increases and approach a constant $1/\sqrt{v_{\tilde{n}_a}}$ for large R_a (see Fig. 4). The phase remains constant in the classically forbidden region and linearly increases with R_a, following $k_{\tilde{n}_a}R_a$, outside the region, as shown in Fig. 5.

Surprisingly, it is found that *the sum of phases of $f_{\tilde{n}_a}$ and $g_{\tilde{n}_a}$ remains unchanged with the value of $\sim 1.5\pi$ in most of the classically forbidden region.* In order to explain this important finding, let us first explain the constancy of the phase of $g_{\tilde{n}_a}$. We consider the flux $\mathcal{F}$ associated with the irregular function $g_{\tilde{n}_a}$:

$$\mathcal{F}(g)=\frac{1}{2i\mu_{A,BC}}\left(g^*_{\tilde{n}_a}(R_a)\frac{dg_{\tilde{n}_a}(R_a)}{dR_a}-\frac{dg^*_{\tilde{n}_a}(R)}{dR_a}g_{\tilde{n}_a}(R_a)\right)$$
$$=\frac{1}{\mu_{A,BC}}[G_{\tilde{n}_a}(R_a)]^2\frac{d}{dR_a}\phi_{\tilde{n}_a}(R_a). \quad (21)$$

Here $G_{\tilde{n}_a}(R_a)$ and $\phi_{\tilde{n}_a}(R_a)$ are, respectively, the magnitude and phase (argument) of $g_{\tilde{n}_a}(R_a)$. Using the asymptotic form of the irregular function $g_{\tilde{n}_a}$ [Eq. (13)] and the flux conservation law, we can see that $\mathcal{F}(g)=1$ at any R_a. Since the magnitude $G_{\tilde{n}_a}(R_a)$ in the classically forbidden region is extremely large, $d\phi_{\tilde{n}_a}(R_a)/dR_a$ must have a very small value. Thus the phase $\phi_{\tilde{n}_a}(R_a)$ is nearly constant in the classically forbidden region.

Let us now determine the value of phase $\phi_{\tilde{n}_a}$ in the classically forbidden region. It is reminded that the irregular function $g_{\tilde{n}_a}$ has the following relation with the regular function $f_{\tilde{n}_a}$ [28]:

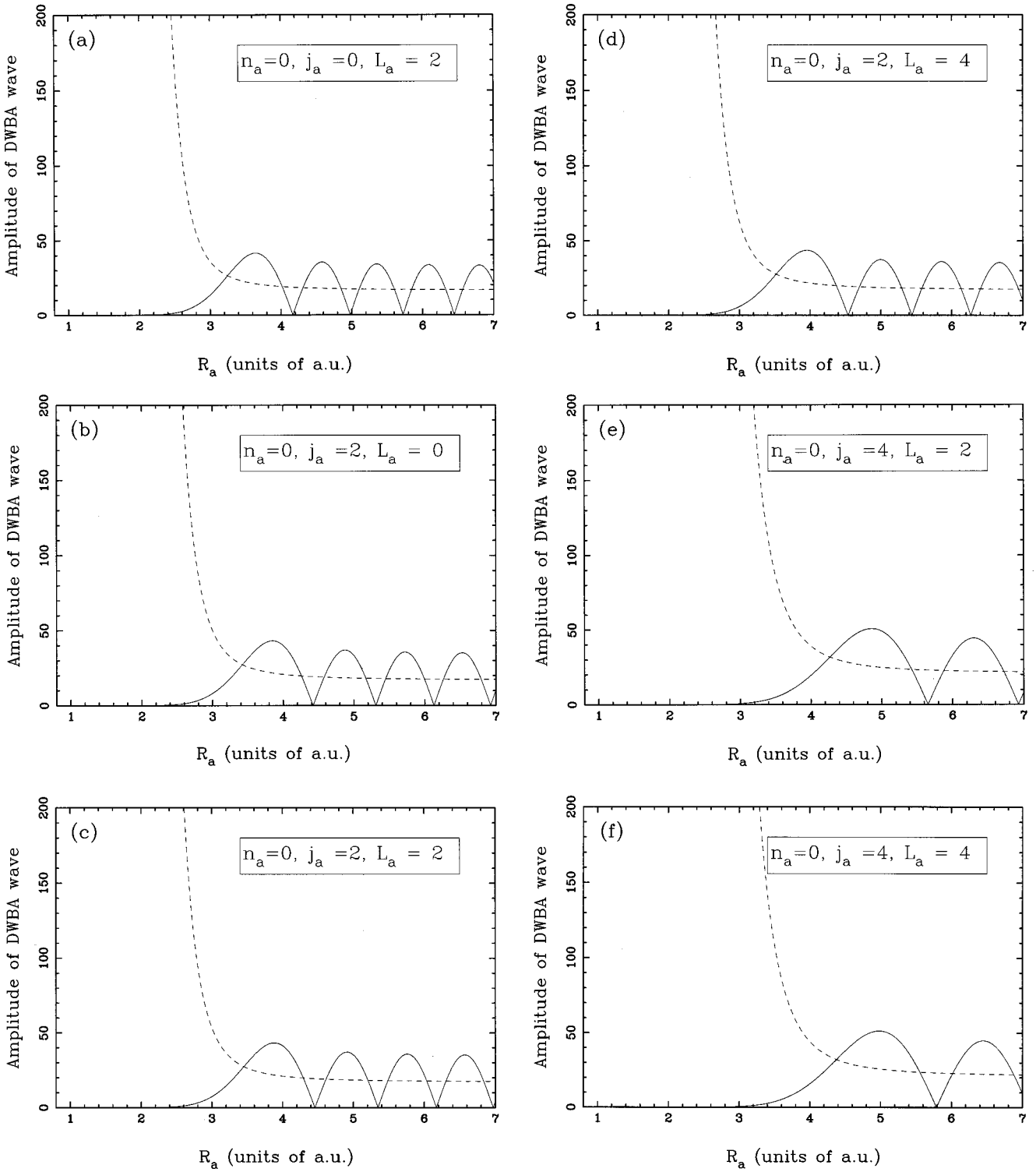

FIG. 4. Amplitudes of regular and irregular wave functions $f_{\tilde{n}_a}$ (solid line) and $g_{\tilde{n}_a}$ (dotted line) in a.u. (a)–(d) correspond to the actively open channels, (e) and (f) the barely open channels, and (g) the closed channel.

$$g_{\tilde{n}_a}(R_a)=f_{\tilde{n}_a}(R_a)\left[W_{\tilde{n}_a}\int_q^{R_a}\frac{1}{f^2_{\tilde{n}_a}(R'_a)}dR'_a+\frac{g_{\tilde{n}_a}(q)}{f_{\tilde{n}_a}(q)}\right], \tag{22}$$

where the point q can be arbitrarily chosen and is taken to be ∞. In the classically forbidden region, the first term on the right-hand side of Eq. (22) is more dominant than the second term. This is because $f^2_{\tilde{n}_a}(R'_a)/W_{\tilde{n}_a}$ is very small in this region. Therefore, we can approximate $g_{\tilde{n}_a}$ as

$$g_{\tilde{n}_a}(R_a)\approx f_{\tilde{n}_a}(R_a)W_{\tilde{n}_a}\int_\infty^{R_a}\frac{1}{f^2_{\tilde{n}_a}(R'_a)}dR'_a. \tag{23}$$

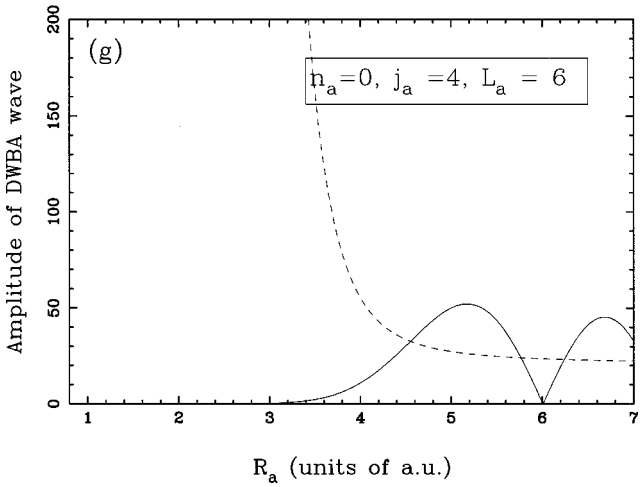

FIG. 4. (*Continued*).

Using the *constant phase shift* $\eta^0_{\tilde{n}_a}$, which is related to $S^0_{\tilde{n}_a,\tilde{n}_a}$ such as $S^0_{\tilde{n}_a,\tilde{n}_a}=e^{2i\eta^0_{\tilde{n}_a}}$, the asymptotic form of $f_{\tilde{n}_a}$ [Eq. (12)] is written as

$$f_{\tilde{n}_a}(R_a)\underset{R_a\to\infty}{\to}\frac{2e^{i(\eta^0_{\tilde{n}_a}+3\pi/2)}}{\sqrt{v_{\tilde{n}_a}}}\sin\left(k_{\tilde{n}_a}R_a-\frac{L_a}{2}\pi+\eta^0_{\tilde{n}_a}\right) \tag{24}$$

for open channels. Hence, in the entire region of R_a, $f_{\tilde{n}_a}(R_a)$ can be expressed as [30]

$$f_{\tilde{n}_a}(R_a)=e^{i\eta_{\tilde{n}_a}}F_{\tilde{n}_a}(R_a), \tag{25}$$

where $\eta_{\tilde{n}_a}=\eta^0_{\tilde{n}_a}+3\pi/2$ and $F_{\tilde{n}_a}$ is the real-valued regular solution of the elastic wave equation $\Delta\cdot\chi=0$, which satisfies the asymptotic boundary condition

$$F_{\tilde{n}_a}\underset{R_a\to\infty}{\to}\frac{2}{\sqrt{v_{\tilde{n}_a}}}\sin\left(k_{\tilde{n}_a}R_a-\frac{L_a}{2}\pi+\eta^0_{\tilde{n}_a}\right). \tag{26}$$

In terms of $F_{\tilde{n}_a}(R_a)$ and $\eta_{\tilde{n}_a}$, Eq. (23) is written as

$$g_{\tilde{n}_a}(R_a)\approx 2\mu_{A,BC}e^{i[(3/2)\pi-\eta_{\tilde{n}_a}]}F_{\tilde{n}_a}(R_a)\int_{R_a}^{\infty}\frac{1}{[F_{\tilde{n}_a}(R'_a)]^2}dR'_a, \tag{27}$$

where we used $W_{\tilde{n}_a}=2\mu_{A,BC}e^{i\pi/2}$ for open channels. Because the sign of $F_{\tilde{n}_a}(R_a)$ in the classically forbidden region does not change as we mentioned above, the phase (argument) of $g_{\tilde{n}_a}$ is given by $\frac{3}{2}\pi-\eta_{\tilde{n}_a}$.

In summary, from the flux conservation law and the fact that the magnitude of $f_{\tilde{n}_a}/\sqrt{\mu_{A,BC}}$ is very small in the classically forbidden region, we find that *the phase* $\phi_{\tilde{n}_a}(R_a)$ *of the irregular function becomes constant with the value of*

$$\phi_{\tilde{n}_a}(R_a)\approx\frac{3}{2}\pi-\eta_{\tilde{n}_a} \tag{28}$$

in this region. By using Eqs. (28), (25), and (11) we clearly see that *the phase of the DW Green's function* $\mathcal{G}^{(+)}_{\tilde{n}_a,\tilde{n}_a}(R_a,R'_a)$ *for the open channel becomes zero when both* R_a *and* R'_a *are in the classically forbidden region.*

Now we examine the property of the first-order perturbation term $\chi^{(1)}=\mathcal{G}^{(+)}V\chi^{0(+)}$ in Eq. (10), which can be explicitly written as

$$\begin{aligned}\chi^{(1)}_{\tilde{n}'_a,\tilde{n}_a}(R_a)&=\tilde{W}_{\tilde{n}'_a}\Bigg[g_{\tilde{n}'_a}(R_a)\int_0^{R_a}f_{\tilde{n}'_a}(R'_a)V_{\tilde{n}'_a,\tilde{n}_a}(R'_a)f_{\tilde{n}_a}(R'_a)dR'_a\\&+f_{\tilde{n}'_a}(R_a)\int_{R_a}^{\infty}g_{\tilde{n}'_a}(R'_a)V_{\tilde{n}'_a,\tilde{n}_a}(R'_a)f_{\tilde{n}_a}(R'_a)dR'_a\Bigg],\end{aligned} \tag{29}$$

where $\tilde{W}_{\tilde{n}_a}=-i$ for the open channels and $\tilde{W}_{\tilde{n}'_a}=-1$ for the closed channels. Note that we focus on $\chi^{(1)}_{\tilde{n}'_a,\tilde{n}_a}(R_a)$ in the range 2.3 a.u.$<R_a<$3.5 a.u.

We study the phase of $\chi^{(1)}_{\tilde{n}'_a,\tilde{n}_a}(R_a)$ for the following three kinds of channels $\tilde{n}'_a$: actively open channels (having relatively large kinetic energy), barely open channels (having substantially small kinetic energy), and closed channels. If $R_{a,turning}<3.5$ a.u., we take $\tilde{n}'_a$ as an actively open channel. In the present example, $\{n'_a=0,j'_a=0,L'_a=2\}$, $\{n'_a=0,j'_a=2,L'_a=0\}$, $\{n'_a=0,j'_a=2,L'_a=2\}$, and $\{n'_a=0,j'_a=2,L'_a=4\}$ are actively open channels, while $\{n'_a=0,j'_a=4,L'_a=2\}$, $\{n'_a=0,j'_a=4,L'_a=4\}$, and $\{n'_a=0,j'_a=4,L'_a=6\}$ are barely open channels (see Fig. 6).

(i) Actively open channels. The deviation of $\phi_{\tilde{n}'_a}(R_a)$ from the constant phase $1.5\pi-\eta_{\tilde{n}_a}$,

$$\Delta\phi_{\tilde{n}'_a}(R_a)=\phi_{\tilde{n}'_a}(R_a)-(1.5\pi-\eta_{\tilde{n}'_a}), \tag{30}$$

starts to increase monotonically near the turning point, being roughly $20°\sim30°$ at $R_a=3.5$ a.u. (see Fig. 5). The channel coupling $V_{\tilde{n}'_a,\tilde{n}_a}$ is found to decrease monotonically in the region $R_a>3.0$ a.u. and to be very small in the region $R_a>4.0$ a.u. (see Fig. 3). Neglecting the contribution of the region 4.0 a.u.$<R_a$ in the second integrand in Eq. (29), we can approximate $\chi^{(1)}_{\tilde{n}'_a,\tilde{n}_a}$ as

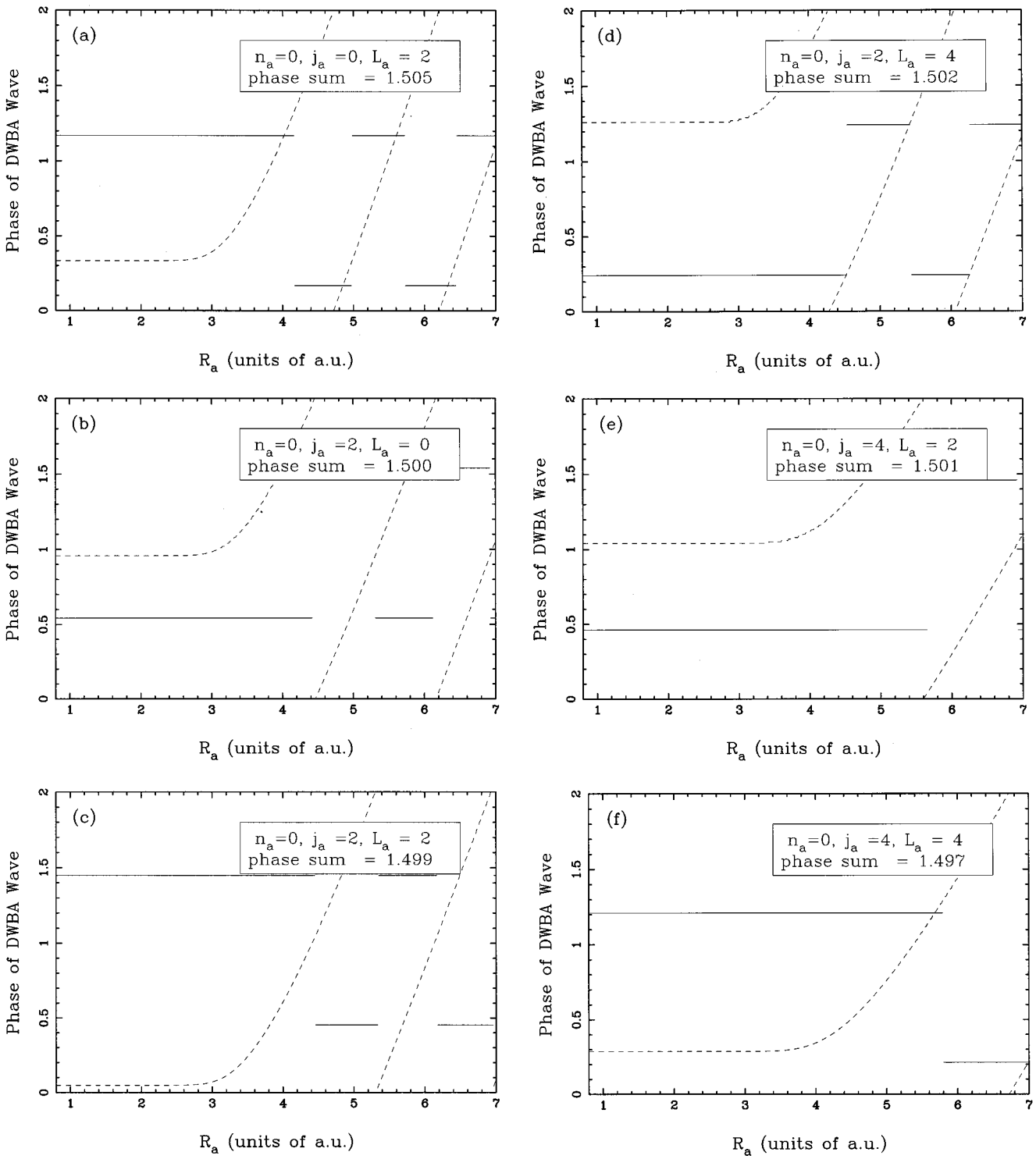

FIG. 5. Phase angles of regular and irregular wave functions $f_{\tilde{n}_a}$ (solid line) and $g_{\tilde{n}_a}$ (dotted line) for the open channels in units of π. The phase sums $\phi_{\tilde{n}_a,g}+\eta_{\tilde{n}_a,f}$ at $R_a=2.0$ a.u. are indicated.

$$\chi^{(1)}_{\tilde{n}'_a,\tilde{n}_a}(R_a)\approx -e^{i\eta_{\tilde{n}_a}}\Bigg[G_{\tilde{n}'_a}(R_a)e^{i\Delta\phi_{\tilde{n}'_a}(R_a)} \times\int_0^{R_a}F_{\tilde{n}'_a}(R'_a)V_{\tilde{n}'_a,\tilde{n}_a}(R'_a)F_{\tilde{n}_a}(R'_a)dR'_a +F_{\tilde{n}'_a}(R_a)\int_{R_a}^{4.0\ \text{a.u.}}e^{i\Delta\phi_{\tilde{n}'_a}(R'_a)}G_{\tilde{n}'_a}(R'_a) V_{\tilde{n}'_a,\tilde{n}_a}(R'_a)F_{\tilde{n}_a}(R'_a)dR'_a\Bigg]. \tag{31}$$

Due to the influence of $\Delta\phi_{\tilde{n}'_a}(R_a)$, the phase of $\chi^{(1)}_{\tilde{n}'_a,\tilde{n}_a}(R_a)$ in the region $R_a<3.5$ a.u. differs from the phase of the entrance channel $\eta_{\tilde{n}_a}$, showing a small variation, with 20°

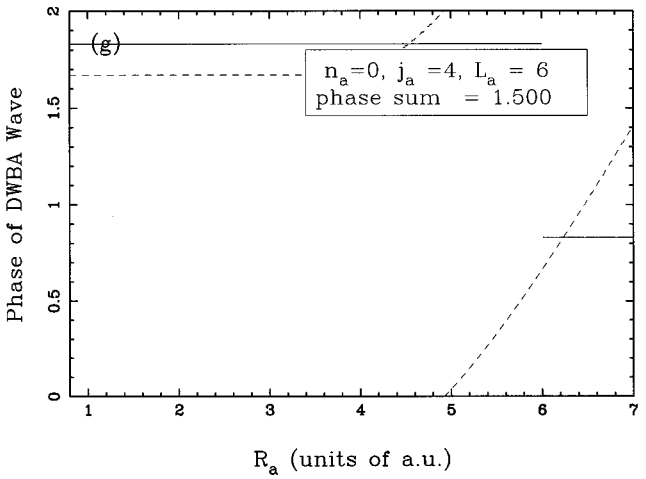

FIG. 5. (*Continued*).

$\sim 30°$ (see Fig. 7). Owing to increment in the magnitude of the phase deviation $\Delta\phi_{\tilde{n}'_a}(R_a)$ as R_a increases, the phase of $\chi^{(1)}_{\tilde{n}'_a}(R_a)$ steadily increases as R_a approaches 4.0 a.u. It is worth noting that *the phases of* $\chi^{(1)}_{\tilde{n}'_a,\tilde{n}_a}(R_a)$ *for the actively open channels are close to each other, showing small deviations from the phase* $\eta_{\tilde{n}_a}$ *of the regular function of the entrance channel*. The magnitude of $\chi^{(1)}_{\tilde{n}'_a,\tilde{n}_a}(R_a)$ in the region $R_a<3.5$ a.u. has a feature similar to that of the entrance channel $f_{\tilde{n}_a}(R_a)$, but the absolute magnitude is about 1/5–1/4 times smaller than that of entrance channel $f_{\tilde{n}_a}(R_a)$ (see Fig. 8). For example, while the maximum amplitude of $f_{\{0,0,2\}}(R_a)$ is 41.47, that of $\chi^{(1)}_{\{0,2,0\},\{0,0,2\}}(R_a)$ is 7.777.

(ii) Barely open channels. For barely open channel the classically forbidden region is wider ($R_a \leqslant 4.3$ a.u.) than that of the actively open channel. Hence the deviation $\Delta\phi_{\tilde{n}'_a}(R_a)\simeq 0$ in the region of interest, as shown in Fig. 5. For example, $\Delta\phi_{\{0,4,2\}}(R_a)=1.8°$ and $\Delta\phi_{\{0,4,6\}}(R_a)=0.0°$ at $R_a=3.5$ a.u. Therefore, as we can see from Eq.(31), the phase of $\chi^{(1)}_{\tilde{n}'_a,\tilde{n}_a}(R_a)$ is nearly the same as that of entrance channel $f_{\tilde{n}_a}(R_a)$ up to π, depending on the sign change of $V_{\tilde{n}'_a,\tilde{n}_a}(R_a)$. In Fig. 7, for example, we can see that the phase of $\chi^{(1)}_{\{0,4,2\},\{0,0,2\}}(R_a)$ is plotted as a nearly solid straight line. The magnitude of $\chi^{(1)}_{\tilde{n}'_a,\tilde{n}_a}(R_a)$ is found to be very small in comparison to those of actively open channels (see Fig. 8). For example, the maximum amplitude of $\chi^{(1)}_{\{0,4,2\},\{0,0,2\}}(R_a)$ is 0.2086. This is due to the weakness of the channel coupling $V_{\tilde{n}'_a,\tilde{n}_a}$ between the barely open channel and the entrance channel, as was mentioned in Sec. IV.

(iii) Closed channels. Since the phases of $f_{\tilde{n}'_a}$ and $g_{\tilde{n}'_a}$ for closed channels are zero, the phases of $\chi^{(1)}_{\tilde{n}'_a,\tilde{n}_a}(R_a)$ are the same as that of entrance channel $f_{\tilde{n}_a}(R_a)$ up to π (by a sign change of the coupling matrix element) (see Fig. 7). However, similarly to the barely open channels, $\chi^{(1)}_{\tilde{n}'_a,\tilde{n}_a}(R_a)$ have much smaller magnitudes (see Fig. 8). For example, the maximum amplitude of $\chi^{(1)}_{\{0,6,4\},\{0,0,2\}}(R_a)$ is 5.096×10^{-3}.

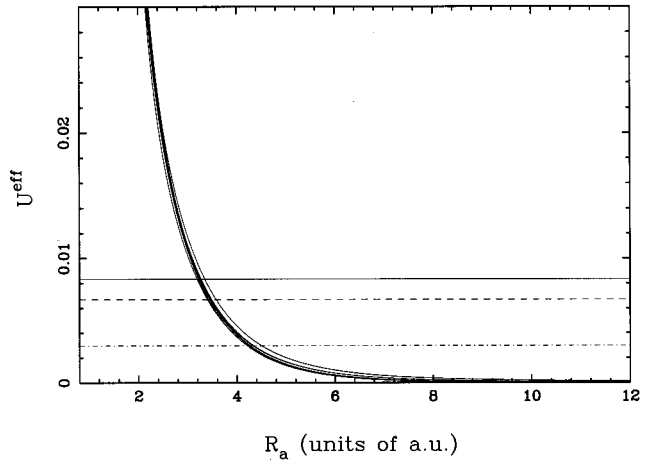

FIG. 6. Effective potentials $U^{eff}_{\tilde{n}_a,\tilde{n}_a}(R_a)$ plotted (solid line) in a.u. The horizontal lines correspond to kinetic energies: The solid line is $\{002\}$, the dashed line $\{020\}$, $\{022\}$, and $\{024\}$, and the dash-dotted line $\{042\}$, $\{044\}$, and$\{046\}$.

Finally, we examine the properties of $\mathcal{G}^{(+)}V\mathcal{G}^{(+)}V\chi^{0(+)}$ and the higher-order terms. The second-order perturbation term $\chi^{(2)}\equiv\mathcal{G}^{(+)}V\mathcal{G}^{(+)}V\chi^{0(+)}=\mathcal{G}^{(+)}V\chi^{(1)}$ in Eq. (10) is written as

$$\chi^{(2)}_{\tilde{n}''_a,\tilde{n}_a}(R_a)=\sum_{\tilde{n}'_a}\tilde{W}_{\tilde{n}''_a}\Bigg[g_{\tilde{n}''_a}(R_a)\int_0^{R_a}f_{\tilde{n}''_a}(R'_a)V_{\tilde{n}''_a,\tilde{n}'_a}(R'_a)\times\chi^{(1)}_{\tilde{n}'_a,\tilde{n}_a}(R'_a)dR'_a+f_{\tilde{n}''_a}(R_a)\int_{R_a}^{\infty}g_{\tilde{n}''_a}(R'_a)V_{\tilde{n}''_a,\tilde{n}'_a}(R'_a)\times\chi^{(1)}_{\tilde{n}'_a,\tilde{n}_a}(R'_a)dR'_a\Bigg]. \tag{32}$$

As was done for the first-order perturbation, we can approximate $\chi^{(2)}_{\tilde{n}''_a,\tilde{n}_a}$ as

$$\chi^{(2)}_{\tilde{n}''_a,\tilde{n}_a}(R_a)\approx -e^{i\eta_{\tilde{n}_a}}\sum_{\tilde{n}'_a}\Bigg[G_{\tilde{n}''_a}(R_a)e^{i\Delta\phi_{\tilde{n}''_a}(R_a)}\times\int_0^{R_a}e^{i\gamma^{(1)}_{\tilde{n}'_a,\tilde{n}_a}(R'_a)}F_{\tilde{n}''_a}(R'_a)V_{\tilde{n}''_a,\tilde{n}'_a}(R'_a)\times\left|\chi^{(1)}_{\tilde{n}'_a,\tilde{n}_a}(R'_a)\right|dR'_a+F_{\tilde{n}''_a}(R_a)\int_{R_a}^{4.0}e^{i\Delta\phi_{\tilde{n}''_a}(R'_a)}\times e^{i\gamma^{(1)}_{\tilde{n}'_a,\tilde{n}_a}(R'_a)}G_{\tilde{n}''_a}(R'_a)V_{\tilde{n}''_a,\tilde{n}'_a}(R'_a)\times\left|\chi^{(1)}_{\tilde{n}'_a,\tilde{n}_a}(R'_a)\right|dR'_a\Bigg], \tag{33}$$

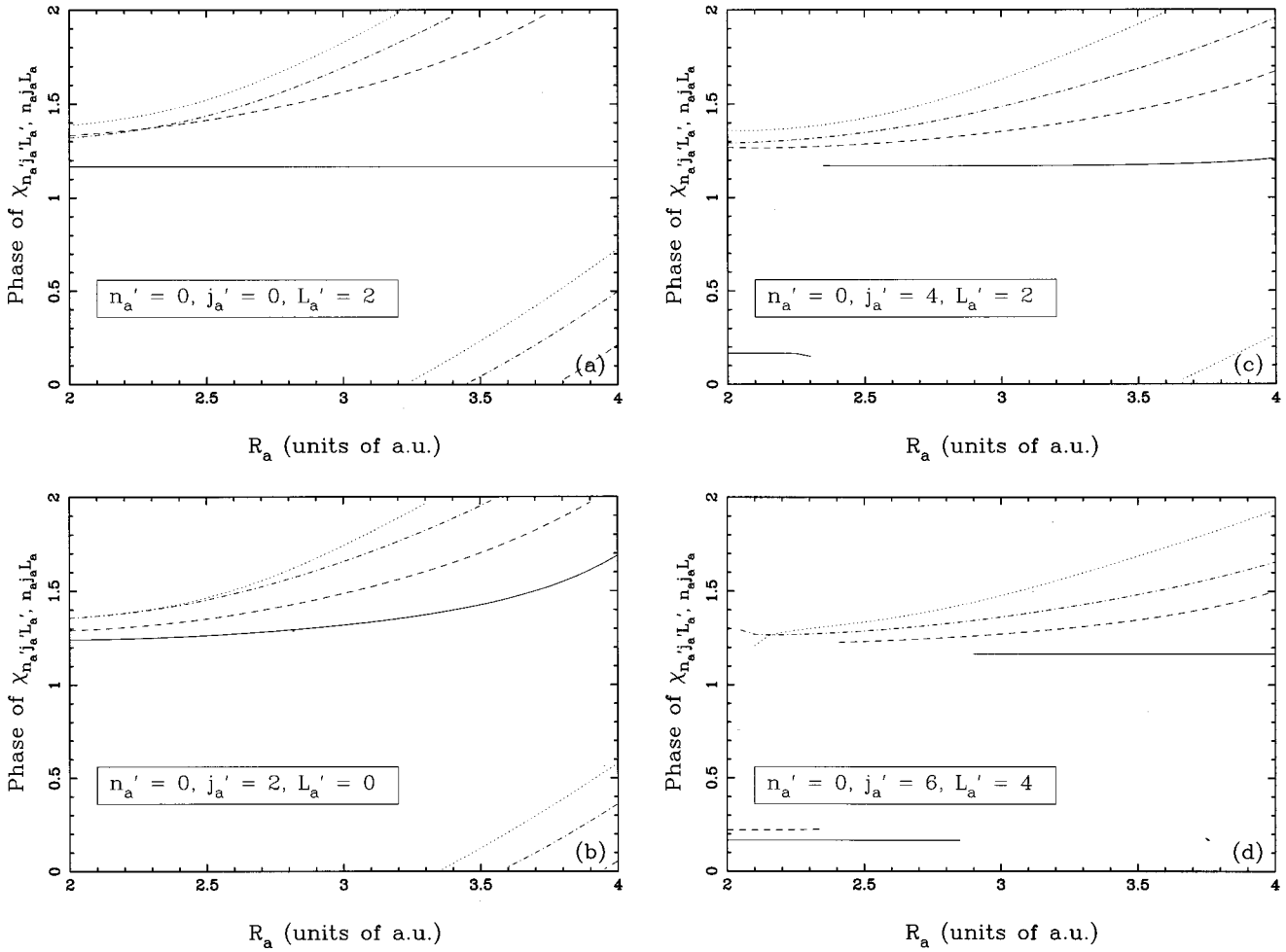

FIG. 7. Phases of $\chi^{(i)}_{\tilde{n}_a',\tilde{n}_a}$ plotted in units of π. The solid line is $\chi^{(1)}_{\tilde{n}_a',\tilde{n}_a}$, the dashed line $\chi^{(2)}_{\tilde{n}_a',\tilde{n}_a}$, the dash-dotted line $\chi^{(3)}_{\tilde{n}_a',\tilde{n}_a}$, and the dotted line $\chi^{(4)}_{\tilde{n}_a',\tilde{n}_a}$. For the $n_a'=0$, $j_a'=0$, and $L_a'=2$ case, the solid line corresponds to the phase of $f_{n_a=0,j_a=0,L_a=2}(R_a)$. The entrance channel is $J=2$, $n_a=0$, $j_a=0$, and $L_a=2$.

where $\gamma^{(1)}_{\tilde{n}_a',\tilde{n}_a}(R_a)$ is the deviation of the phase (argument) $\eta^{(1)}_{\tilde{n}_a',\tilde{n}_a}(R_a)$ of $\chi^{(1)}_{\tilde{n}_a',\tilde{n}_a}(R_a)$ from the constant phase $\eta_{\tilde{n}_a}$ of the DW $\chi^{(0)}_{\tilde{n}_a,\tilde{n}_a}(R_a)$,

$$\gamma^{(1)}_{\tilde{n}_a',\tilde{n}_a}(R_a)=\eta^{(1)}_{\tilde{n}_a',\tilde{n}_a}(R_a)-\eta_{\tilde{n}_a}. \tag{34}$$

For the actively open channel $\tilde{n}_a'$, $\gamma^{(1)}_{\tilde{n}_a',\tilde{n}_a}(R_a)$ is nearly constant with the phase angle of 20°–30° for $R_a<3.0$ a.u. and slowly increases as $R_a\rightarrow 4.0$ a.u., while for barely open and closed channels $\tilde{n}_a'$, $\gamma^{(1)}_{\tilde{n}_a',\tilde{n}_a}(R_a)\simeq 0$ (see the solid lines in Fig. 7). For example, $\gamma^{(1)}_{\{0,2,0\},\{0,0,2\}}(R_a)=27.43°$ at $R_a=3.0$ a.u. and 49.46° at $R_a=3.5$ a.u. (this is an actively open channel) and $\gamma^{(1)}_{\{0,4,2\},\{0,0,2\}}(R_a)=1.458°$ at $R_a=3.5$ a.u. (this is a barely open channel).

(a) Actively open channels. For the actively open channel $\tilde{n}_a''$, by the effects of $\Delta\phi_{\tilde{n}_a''}(R_a)$ and $\gamma^{(1)}_{\tilde{n}_a',\tilde{n}_a}(R_a)$, the argument of $\chi^{(2)}_{\tilde{n}_a'',\tilde{n}_a}(R_a)$ is noticeably changed from that of $\chi^{(1)}_{\tilde{n}_a'',\tilde{n}_a}(R_a)$, the difference of phases between $\chi^{(2)}_{\tilde{n}_a'',\tilde{n}_a}(R_a)$ and $\chi^{(1)}_{\tilde{n}_a'',\tilde{n}_a}(R_a)$ being about 50° at $R_a=3.5$ a.u. As R_a increases, the phase increases more rapidly than that of $\chi^{(1)}_{\tilde{n}_a'',\tilde{n}_a}(R_a)$ (see Fig. 7). However, the magnitude of $\chi^{(2)}_{\tilde{n}_a'',\tilde{n}_a}(R_a)$ diminishes and becomes smaller (about 1/5 times) compared to that of $\chi^{(1)}_{\tilde{n}_a'',\tilde{n}_a}(R_a)$ (see Fig. 8). Therefore, the sum $\chi^{(1)}_{\tilde{n}_a'',\tilde{n}_a}(R_a)+\chi^{(2)}_{\tilde{n}_a'',\tilde{n}_a}(R_a)$ is changed only a little from $\chi^{(1)}_{\tilde{n}_a'',\tilde{n}_a}(R_a)$ (see Figs. 9 and 10). That is, the argument (phase) of $\chi^{(1)}_{\tilde{n}_a'',\tilde{n}_a}\times(R_a)+\chi^{(2)}_{\tilde{n}_a'',\tilde{n}_a}(R_a)$ is close to the phase $\eta^{(1)}_{\tilde{n}_a',\tilde{n}_a}$ of the first-order perturbation term, which shows a small deviation $\gamma^{(1)}_{\tilde{n}_a',\tilde{n}_a}$ from $\eta_{\tilde{n}_a}$.

(b) Barely open and closed channels. Since the barely open and closed channels are far from the entrance channel, the second-order perturbations mediated by the actively open channels $\tilde{n}_a'$ lying between $\tilde{n}_a''$ and $\tilde{n}_a$ are larger than the first-order perturbations arising from the direct couplings. As can be seen from Fig. 8, for the barely open and closed channels, the magnitude of $\chi^{(2)}_{\tilde{n}_a'',\tilde{n}_a}(R_a)$ is larger by about 5–8 times than that of $\chi^{(1)}_{\tilde{n}_a'',\tilde{n}_a}(R_a)$. $\Delta\phi_{\tilde{n}_a''}(R_a)\approx 0$ for the

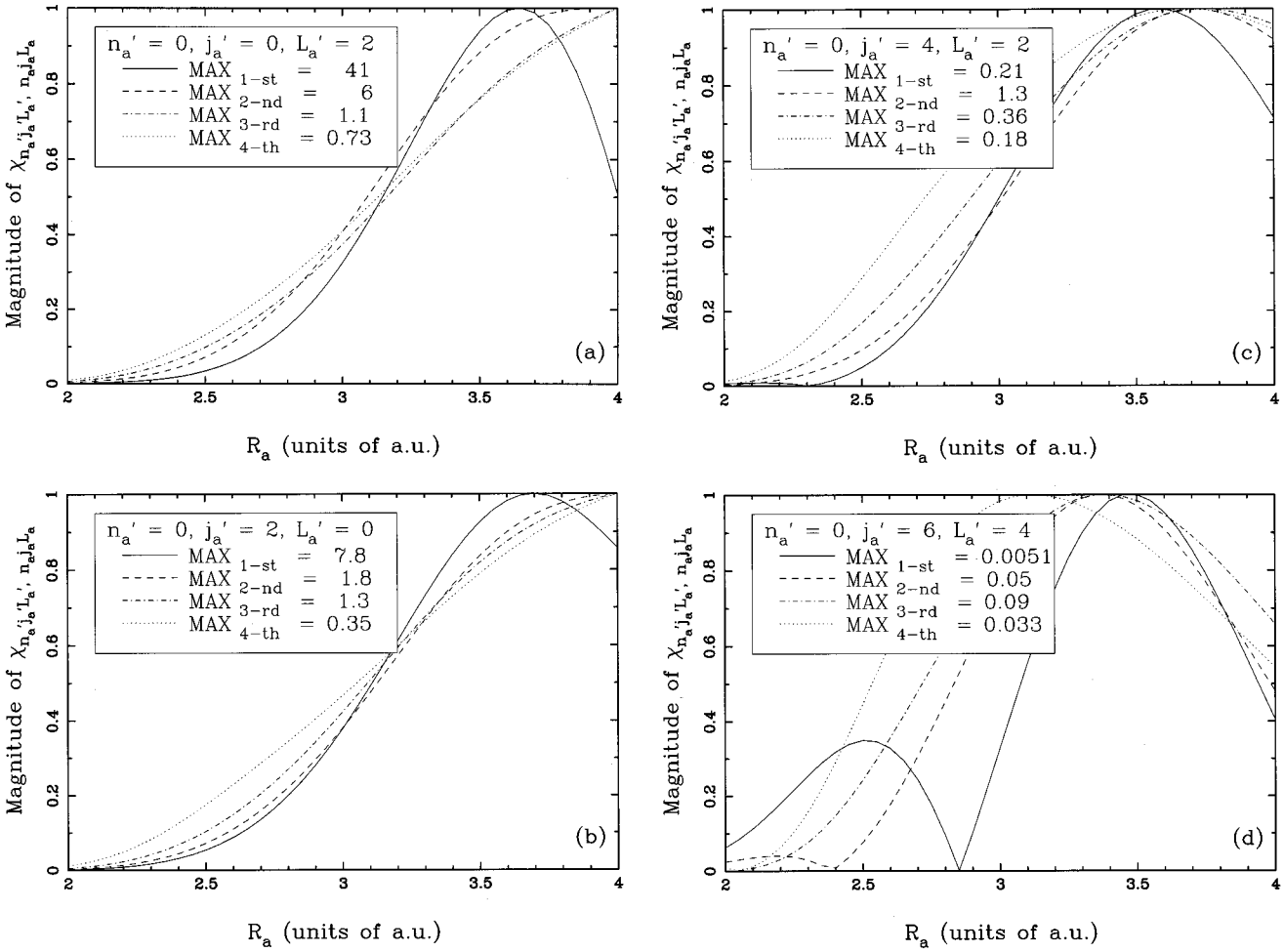

FIG. 8. Normalized amplitudes of $\chi^{(i)}_{\tilde{n}'_a,\tilde{n}_a}$ are plotted in a.u. The maximum values are presented. The solid line is $\chi^{(1)}_{\tilde{n}'_a,\tilde{n}_a}$, the dashed line $\chi^{(2)}_{\tilde{n}'_a,\tilde{n}_a}$, the dash-dotted line $\chi^{(3)}_{\tilde{n}'_a,\tilde{n}_a}$, and the dotted line $\chi^{(4)}_{\tilde{n}'_a,\tilde{n}_a}$. For the $n'_a=0$, $j'_a=0$, and $L'_a=2$ case, the solid line corresponds to $f_{n_a=0,j_a=0,L_a=2}(R_a)$. The entrance channel is $J=2$, $n_a=0$, $j_a=0$, and $L_a=2$.

barely open and closed channels $\tilde{n}''_a$, as was mentioned above. Thus, from Eq. (33), we can be see that the phase of $\chi^{(2)}_{\tilde{n}''_a,\tilde{n}_a}(R_a)$ is mainly affected by the deviations $\gamma^{(1)}_{\tilde{n}'_a,\tilde{n}_a}$ of the actively open channels $\tilde{n}'_a$. Since the deviations $\gamma^{(1)}_{\tilde{n}'_a,\tilde{n}_a}$ for the actively open channels $\tilde{n}'_a$ are nearly all the same and are slowly increasing (i.e., nearly constant) functions of R_a, the phase of $\chi^{(2)}_{\tilde{n}''_a,\tilde{n}_a}(R_a)$ becomes close to the phases $\eta^{(1)}_{\tilde{n}'_a,\tilde{n}_a}$ of the first-order CC waves. For example, in Fig. 7 we can see that the phase of $\chi^{(2)}_{\{0,4,2\},\{0,0,2\}}$ is very close to the phase of $\chi^{(1)}_{\{0,2,0\},\{0,0,2\}}$. Thus the phase of $\chi^{(1)}_{\tilde{n}''_a,\tilde{n}_a}(R_a)+\chi^{(2)}_{\tilde{n}''_a,\tilde{n}_a}(R_a)$, which is determined mainly by the second-order perturbation term $\chi^{(2)}_{\tilde{n}''_a,\tilde{n}_a}(R_a)$, is close to the phases of the first-order perturbation term $\chi^{(1)}_{\tilde{n}'_a,\tilde{n}_a}(R_a)$ for the actively open channels $\tilde{n}'_a$, which mediate between the barely open (or closed) channel $\tilde{n}''_a$ and the entrance channel $\tilde{n}_a$. In Fig. 9 we can see that the phases of $\chi^{(1)}_{\{0,4,2\},\{0,0,2\}}+\chi^{(2)}_{\{0,4,2\},\{0,0,2\}}$ and $\chi^{(1)}_{\{0,6,4\},\{0,0,2\}}+\chi^{(2)}_{\{0,6,4\},\{0,0,2\}}$ are very similar to the phase of $\chi^{(1)}_{\{0,2,0\},\{0,0,2\}}$.

(c) Higher-order terms. For the higher-order perturbation terms, we can argue with the same logic as discussed above. For an actively open channel $\tilde{n}'_a$, the higher-order perturbation terms are negligible compared to the first-order term $\chi^{(1)}_{\tilde{n}'_a,\tilde{n}_a}$ and the CC wave $\chi_{\tilde{n}'_a,\tilde{n}_a}$ in Eq. (10) converges well with the inclusion of only about four or five perturbation terms. Hence the phase of $\chi_{\tilde{n}'_a,\tilde{n}_a}$ is close to that of $\chi^{(1)}_{\tilde{n}'_a,\tilde{n}_a}$. On the other hand, for a closed (or barely open) channel $\tilde{n}''_a$, the most contributive perturbation terms correspond to the multistep couplings in which the intermediate channels are coupled with their nearest channels at each step. For example, for the closed channel $\tilde{n}''_a=\{0,6,4\}$, the third-order perturbation term is the most contributive one, which results from the multistep couplings $\{0,0,2\}\rightarrow\{0,2,2\}\rightarrow\{0,4,2\}\rightarrow\{0,6,4\}$, $\{0,0,2\}\rightarrow\{0,2,2\}\rightarrow\{0,4,4\}\rightarrow\{0,6,4\}$, $\{0,0,2\}\rightarrow\{0,2,0\}\rightarrow\{0,4,2\}\rightarrow\{0,6,4\}$, $\{0,0,2\}\rightarrow\{0,2,4\}\rightarrow\{0,4,2\}\rightarrow\{0,6,4\}$, and $\{0,0,2\}\rightarrow\{0,2,4\}\rightarrow\{0,4,4\}\rightarrow\{0,6,4\}$. It should be noted that only one actively open channel is involved in each multistep coupling as an intermediate channel. Thus the phase of $\chi_{\tilde{n}''_a,\tilde{n}_a}$ is close to the phase of the first-order perturbation term $\chi^{(1)}_{\tilde{n}''_a,\tilde{n}_a}$ for the intermediate actively open channel $\tilde{n}'_a$. For the closed (or barely open)

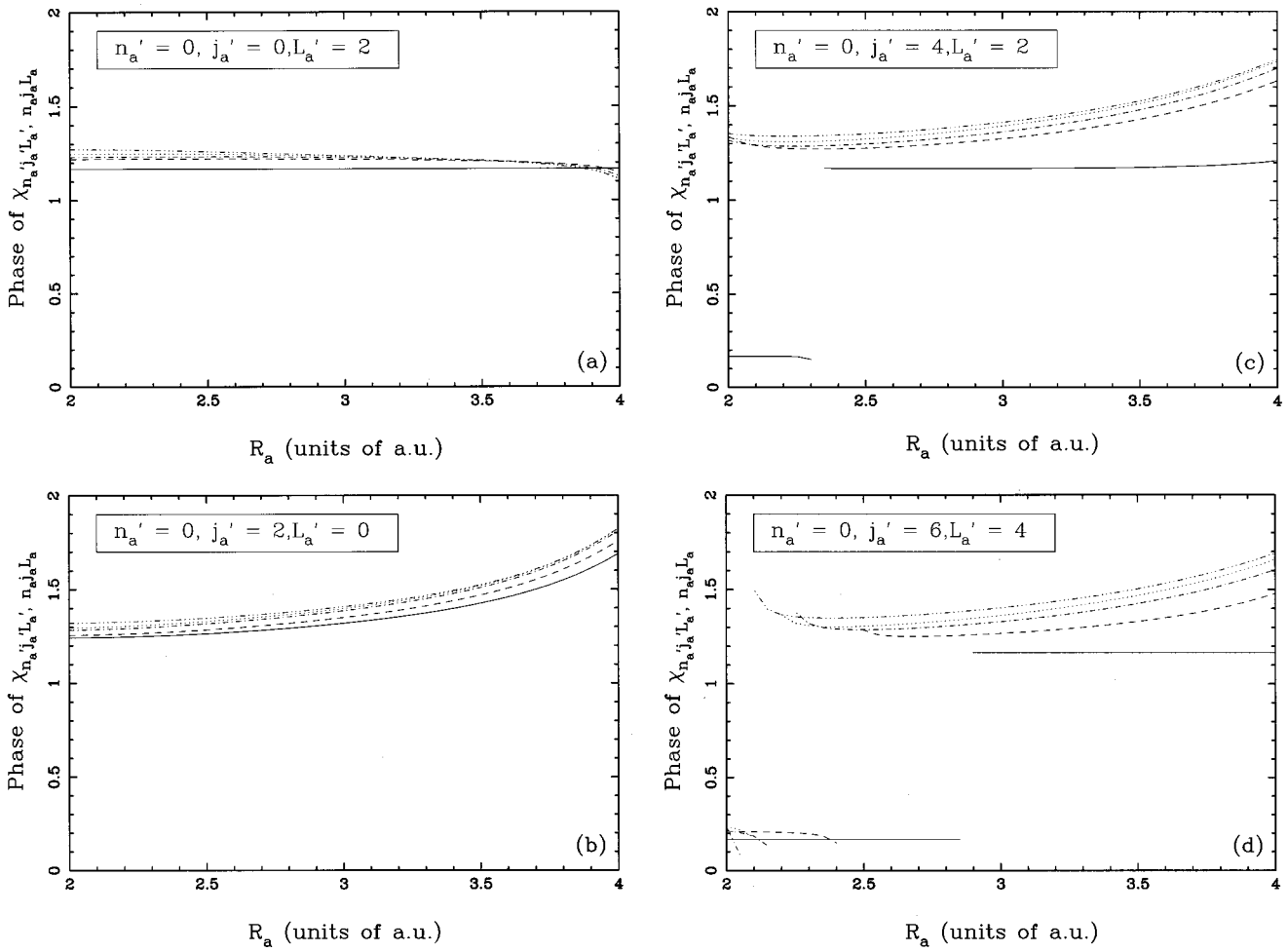

FIG. 9. Phase angles of $\chi^{(i)}_{\tilde{n}'_a,\tilde{n}_a}$ plotted in units of π. The solid line is $\chi^{(1)}_{\tilde{n}'_a,\tilde{n}_a}$, the dashed line $\chi^{(1)}_{\tilde{n}'_a,\tilde{n}_a}+\chi^{(2)}_{\tilde{n}'_a,\tilde{n}_a}$, the dash-dotted line $\chi^{(1)}_{\tilde{n}'_a,\tilde{n}_a}+\chi^{(2)}_{\tilde{n}'_a,\tilde{n}_a}+\chi^{(3)}_{\tilde{n}'_a,\tilde{n}_a}$, the dotted line $\chi^{(1)}_{\tilde{n}'_a,\tilde{n}_a}+\cdots+\chi^{(4)}_{\tilde{n}'_a,\tilde{n}_a}$, and the dash-dot-dot-dotted line, $\chi^{(1)}_{\tilde{n}'_a,\tilde{n}_a}+\cdots+\chi^{(10)}_{\tilde{n}'_a,\tilde{n}_a}$. The entrance channel is $J=2$, $n_a=0$, $j_a=0$, and $L_a=2$. The solid line of the first figure (a) is the phase of $f_{n_a=0,j_a=0,L_a=2}(R_a)$.

channels $\tilde{n}''_a$, the $\chi_{\tilde{n}''_a,\tilde{n}_a}$ in Eq. (10) converge well with the inclusion of ten perturbation terms.

Finally, for a given entrance channel $\tilde{n}_a$, the phases of the the first-order perturbation terms $\chi^{(1)}_{\tilde{n}'_a,\tilde{n}_a}$ for the actively open channels $\tilde{n}'_a$ are nearly all the same, showing only small deviations from the phase of the DW $\chi^{(0)}_{\tilde{n}_a,\tilde{n}_a}$. The phase of $\chi_{\tilde{n}'_a,\tilde{n}_a}$ for any channel $\tilde{n}'_a$ is close to the phases of the first-order perturbation terms for the actively open channels. Hence *the phase of $\chi_{\tilde{n}'_a,\tilde{n}_a}$ is nearly independent of the channels $\tilde{n}'_a$ and is close to that of the distorted-wave for the entrance channel $\tilde{n}_a$, showing only a small deviation.* It is remarkable to note that the propensity of phase variation with channel members (n_a,J,L_b,L_a) is identical for both the CCBA and DWBA results, as shown in Tables I and II.

VI. SUMMARY

By paying attention to the dynamic phases of the CC wave functions, we have presented physical interpretations on the cause of agreement in the structure of the angular distributions between the CCBA and DWBA, which are concerned with rearrangement collisions at low energies. Specifically the phases of CC wave functions were examined and compared with the phase of the elastic (single-channel) DW function. We found that the CC wave functions $\chi^{J}_{\tilde{n}'_a,\tilde{n}_a}$ near the classically forbidden region 2.3 a.u.$<R_a<$3.5 a.u. dominantly contribute to the transition amplitude. In low-energy collision processes the phases of CC wave functions are close to the constant phase $\eta_{\tilde{n}_a}$ of the elastic channel, particularly in the classically forbidden region. This is the cause of agreement between the CCBA and DWBA. It is crucial for the understanding of the constancy of the CC wave phases that the phase of the irregular function $g_{\tilde{n}_a}$ in the classically forbidden region is nearly constant with the value $3/2\pi-\eta_{\tilde{n}_a}$. It is important to realize that the memory of initial (final) phase of the entrance (exit) channel is not lost during the reactive scattering process and as a consequence the structure of the angular distributions is not modified by the (nonreactive) channel coupling in the low-energy collision process.

However, at higher energies (e.g., above 0.7 eV for the H_3 system) the DWBA treatment should be avoided, as such a

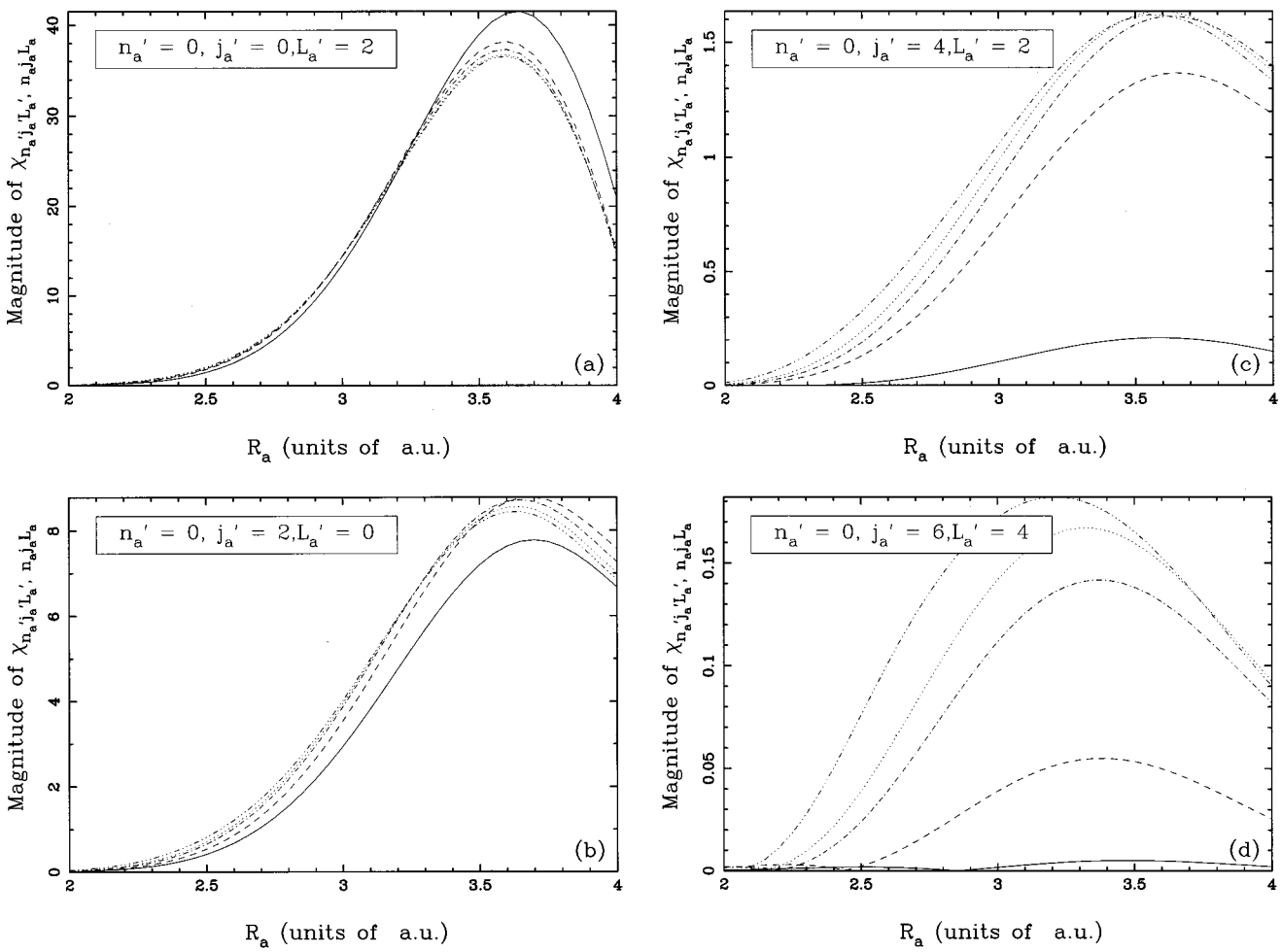

FIG. 10. The amplitudes of $\chi^{(i)}_{\tilde{n}'_a,\tilde{n}_a}$ are plotted in the unit of a.u. The solid line is $\chi^{(1)}_{\tilde{n}'_a,\tilde{n}_a}$, the dashed line $\chi^{(1)}_{\tilde{n}'_a,\tilde{n}_a}+\chi^{(2)}_{\tilde{n}'_a,\tilde{n}_a}$, the dash-dotted line $\chi^{(1)}_{\tilde{n}'_a,\tilde{n}_a}+\chi^{(2)}_{\tilde{n}'_a,\tilde{n}_a}+\chi^{(3)}_{\tilde{n}'_a,\tilde{n}_a}$, the dotted line $\chi^{(1)}_{\tilde{n}'_a,\tilde{n}_a}+\cdots+\chi^{(4)}_{\tilde{n}'_a,\tilde{n}_a}$, and the dash–triple-dotted line $\chi^{(1)}_{\tilde{n}'_a,\tilde{n}_a}+\cdots+\chi^{(10)}_{\tilde{n}'_a,\tilde{n}_a}$. The entrance channel is $J=2$, $n_a=0$, $j_a=0$, and $L_a=2$. The solid line of (a) is the magnitude of $f_{n_a=0,j_a=0,L_a=2}(R_a)$.

memory effect will be lost. The reactive zone of interest, that is, the most contributive zone to the transition amplitude, becomes larger in area, by covering the region beyond the classical forbidden region in which the phases of actively open channels are no longer the same as that of the entrance channel. Further, the number of actively open channels increases with collision energy and channel-coupling effects will be increasingly important to allow for a large difference in phases between the entrance channel and the intermediate channels. This is the main reason why the DWBA fails to predict even the relative angular distributions at higher energies.

The magnitude distributions of $T^J_{n_a j_a L_a n_b j_b L_b}$ are, of course, important to the determination of the structure of the angular distributions. We plan to discuss it elsewhere later.

ACKNOWLEDGMENTS

This work was supported in part by the Center for Molecular Science at KAIST and by the Research Fund of Kumoh National University of Technology. One of us (S.H.S.S.) acknowledges the partial financial support of a BSRI project. Most of the numerical calculations were performed on the CRAY-C90 computer at the System Engineering Research Institute.

[1] A. Kuppermann and G. C. Schatz, J. Chem. Phys. **62**, 2502 (1976); G. C. Schatz and A. Kuppermann, *ibid.* **65**, 4642 (1976).

[2] A. B. Elkowitz and R. E. Wyatt, J. Chem. Phys. **62**, 2504 (1975); **63**, 702 (1975).

[3] R. T. Pack and G. A. Parker, J. Chem. Phys. **87**, 3888 (1987).

[4] W. H. Miller, *Methods in Computational Molecular Physics*, edited by Stephen Wilson and G. H. F. Diercksen (Plenum, New York, 1992); and references therein.

[5] D. E. Manolopoulos and R. E. Wyatt, Chem. Phys. Lett. **152**, 23 (1988).

[6] T. Seideman and W. H. Miller, J. Chem. Phys. **97**, 2499 (1992).

[7] W. H. Miller, J. Chem. Phys. **49**, 2373 (1968).

[8] R. D. Levind, Isr. J. Chem. **8**, 13 (1970).
[9] K. T. Tang and M. Karplus, Phys. Rev. A **4**, 1844 (1971).
[10] S. H. Suck Salk, Phys. Rev. A **15**, 1893 (1977).
[11] T. Tamura, Phys. Rep. **14**, 59 (1974), and references therein.
[12] S. H. Suck Salk, Phys. Rev. A **27**, 187 (1983).
[13] L. M. Hubbard, S.-H. Shi, and W. H. Miller, J. Chem. Phys. **78**, 2381 (1983).
[14] G. C. Schatz, L. M. Hubbard, P. S. Dardi, and W. H. Miller, J. Chem. Phys. **81**, 231 (1984).
[15] B. H. Choi, R. T. Poe, and K. T. Tang, J. Chem. Phys. **81**, 4979 (1984).
[16] R. T. Pack, J. Chem. Phys. **60**, 633 (1974).
[17] *Theory of Chemical Reaction Dynamics*, edited by M. Baer (CRC, Boca Raton, FL, 1985), Vol. I–IV.
[18] N. N. Choi and Sung-Hosuck Salk, Phys. Rev. A **53**, 785 (1996); S. H. Suck Salk and R. W. Emmons, *ibid.* **24**, 129 (1981).
[19] P. Halvick, M. Zhao, D. G. Truhlar, D. W. Schwenke, and D. J. Kouri, J. Chem. Soc. Faraday Trans. **86**, 1705 (1990), and references therein.
[20] S. H. Suck Salk and C. K. Lutrus, J. Chem. Phys. **83**, 3965 (1985).
[21] S. H. Suck Salk, C. R. Klein, and C. K. Lutus, Chem. Phys. Lett. **110**, 112 (1984).
[22] M. Nakamura, J. Chem. Phys. **95**, 4102 (1991).
[23] S. H. Suck Salk, Phys. Rev. C **43**, 812 (1991); Phys. Rev. A **32**, 2670 (1985).
[24] N. N. Choi, M.-H. Lee, and S. H. Suck Salk, J. Korean Phys. Soc. **32**, 425 (1998).
[25] R. N. Porter and M. Karplus, J. Chem. Phys. **40**, 1105 (1964).
[26] D. A. Varshalovich, A. N. Moskalev, and V. K. Khersonskii, *Quantum Theory of Angular Momentum* (World Scientific, Singapore, 1988).
[27] A. R. Edmonds, *Angular Momentum in Quantum Mechanics* (Princeton University Press, Princeton, 1974).
[28] G. Arfken, *Mathematical Methods for Physics* (Academic, Orlando, 1985).
[29] P. S. Dardi, S. Shi, and W. H. Miller, J. Chem. Phys. **83**, 575 (1985).
[30] R. G. Newton, *Scattering Theory of Waves and Particles* (Springer-Verlag, New York, 1982), Chap. 11.